Closed-Loop Continuous Hand Control via Chronic Recording of Regenerative Peripheral Nerve Interfaces

Philip P. Vu, *Student Member, IEEE*, Zachary T. Irwin, *Student Member, IEEE*, Autumn J. Bullard, Shoshana W. Ambani, Ian C. Sando, Melanie G. Urbanchek, *Member, IEEE*, Paul S. Cederna, and Cynthia A. Chestek, *Member, IEEE*

***Abstract*— Loss of the upper limb imposes a devastating interruption to everyday life. Full restoration of natural arm control requires the ability to simultaneously control multiple degrees of freedom of the prosthetic arm and maintain that control over an extended period of time. Current clinically available myoelectric prostheses do not provide simultaneous control or consistency for transradial amputees. To address this issue, we have implemented a standard Kalman filter for continuous hand control using intramuscular electromyography (EMG) from both regenerative peripheral nerve interfaces (RPNI) and an intact muscle within non-human primates. Seven RPNIs and one intact muscle were implanted with indwelling bipolar intramuscular electrodes in two rhesus macaques. Following recuperations, function-specific EMG signals were recorded and then fed through the Kalman filter during a hand-movement behavioral task to continuously predict the monkey's finger position. We were able to reconstruct continuous finger movement offline with an average correlation of $\rho = 0.87$ and a root mean squared error (RMSE) of 0.12 between actual and predicted position from two macaques. This finger movement prediction was also performed in real time to enable closed-loop neural control of a virtual hand. Compared with physical hand control, neural control performance was slightly slower but maintained an average target hit success rate of 96.70%. Recalibration longevity measurements maintained consistent average correlation over time but had a significant change in RMSE ($p < 0.05$). Additionally, extracted single units varied in amplitude by a factor of +18.65% and −25.85% compared with its mean. This is the first demonstration of chronic indwelling electrodes being used for continuous position control via the Kalman filter. Combining these analyses with our novel peripheral nerve interface, we believe that this demonstrates an important step in providing patients with more naturalistic control of their prosthetic limbs.**

***Index Terms*— Intramuscular electromyography, myoelectric prostheses, peripheral nerve, implantable electrodes.**

Manuscript received March 17, 2017; revised August 5, 2017; accepted October 12, 2017. Date of publication November 13, 2017; date of current version February 9, 2018. This work was supported in part by the Wallace H. Coulter Foundation, in part by the Plastic Surgery Foundation, and in part by the Frederick A. Coller Surgical Society. The work of P. P. Vu and A. J. Bullard was supported by the NSF Graduate Research Fellowships. *(Corresponding author: Philip P. Vu.)*

P. P. Vu, Z. T. Irwin, A. J. Bullard, and C. A. Chestek are with the Biomedical Engineering Department, University of Michigan, Ann Arbor, MI 48109 USA (e-mail: philipv@umich.edu; cchestek@umich.edu).

S. W. Ambani, I. C. Sando, and M. G. Urbanchek are with the Plastic Surgery Section, Department of Surgery, University of Michigan, Ann Arbor, MI 48109 USA.

P. S. Cederna is with the Biomedical Engineering Department and the Plastic Surgery Section, Department of Surgery, University of Michigan, Ann Arbor, MI 48109 USA.

Digital Object Identifier 10.1109/TNSRE.2017.2772961

I. Introduction

LIMB loss can have a significant negative impact on a person's daily life. Every year, around 185,000 people will undergo some sort of amputation, [1] and the current number of people living with an amputation may increase by a factor of 10 within the next 3-4 years [2]. The loss is particularly devastating in the case of upper limb amputation. As one possible solution, myoelectric prosthesis technology can help assist these people and alleviate their daily struggles. Myoelectric prostheses work by using electromyogram (EMG) signals from residual muscle to control prosthetic hand movements. However, despite the improved hardware and functionality of prosthesis technology within the past decade, an adequate control strategy is ultimately lacking [3]. Current control strategies involve two muscle activations controlling multiple functions of the prosthetic hand. For example, flexing and extending the wrist muscle would control the prosthetic wrist flex/extend function and also the hand open/close function. Users would switch between functions through co-contracting the flexion and extension muscles, or another mode selection mechanism. Three main components of this current control strategy make clinical myoelectric prosthetics unappealing to patients: the unintuitive feeling of control, the low level of performance and movement complexity compared to the natural hand, and the amount of training time it takes to achieve even that limited amount of performance.

To address some of these issues, current research has focused on improving these discrete classification algorithms to achieve higher performance and provide a more intuitive control mechanism. Discrete machine learning algorithms classify different movements based on patterns of EMG signal features, allowing users to directly select a movement to perform rather than having to switch modes. Recent advancements have led to an increased number of

classified posture movements, i.e. wrist flex/extend, forearm pronation/supination, and radial/ulnar deviation [4], [5], [6] with further studies using EMG feature patterns to control individual fingers and finger combinations [7]–[9]. Discrete classifiers have achieved $> 90\%$ decoding accuracy in both able-bodied participants [4], [5] and transradial amputee subjects [8], [10], [11], [12]. This has overall granted myoelectric users with multi-functionality and a slightly more intuitive control scheme.

Despite the high classification accuracy, certain characteristics of discrete classifiers prevent them from becoming the end-all solution for myoelectric prosthetic control. Classifiers can only operate sequentially and cannot provide simultaneous control for more complex movements. If the user desired to rotate the wrist and open the hand at the same time, an additional class would need to be trained. This would result in increased training time and may be impractical in a clinical setting. Additionally, classifiers inherently do not provide proportional control, acting only in a binary on/off basis. The ability to control the speed and strength of the prosthesis is necessary for more refined tasks. Thus, the absence of simultaneous and proportional characteristics limits the overall level of natural control a discrete classifier can provide.

Regression algorithms, on the other hand, can offer both proportional and simultaneous control. They have the ability to continuously predict the output of multiple movement signals and provide users with a more intuitive control scheme. Several groups have demonstrated simultaneous and proportional control of wrist flex/extend, wrist supination/pronation, ulnar and radial deviation and hand open/close from EMG signals in both able-bodied and transradial amputee subjects [13]–[15]. However, very few studies have focused on restoring continuous control of individuated fingers using EMG, with the exception of those using neural networks to estimate joint finger angles in able-bodied subjects [16], [17]. More investigation is needed in improving regression algorithms to control finger movements using EMG signals. In addition, the regression studies mentioned above used surface EMG signals, which cannot record EMG from specific muscles and has signal stability challenges such as movement artifacts, skin impedance changes, and electrode shifts. To overcome these issues, intramuscular EMG recordings may provide a more stable and more localized signal for regression algorithms. Smith *et al.* [18], has demonstrated that intramuscular EMG can be used in regression algorithms to control wrist flex/extend, wrist supination/pronation, and hand open/close in able-bodied and amputee subjects. This holds promise for future studies to explore the specificity of intramuscular EMG for fine finger movements.

However, an additional concern for these novel regression algorithms is that they cannot be used when the necessary muscles are missing. Every person with an amputation is missing some amount of muscle, whether it is intrinsic hand function alone for a distal transradial amputee or complete loss of hand control in a transhumeral amputee. To address this, several groups have explored interfacing with the peripheral nerves in the residual limb of amputee patients for prosthetic hand control [19]–[22]. Utah Slanted Electrode Arrays (USEA), intrafascicular electrodes, have been implanted into the median and ulnar nerve of two subjects with previous transradial amputations [19]. Using a Kalman filter, a linear regression based algorithm, Davis *et al.* [19] were able to continuously estimate finger position based on the firing rates of multiple neurons recorded from the USEA. Although promising, the group also reported a significant reduction in signal strength within the 1 month period of implantation. Most other groups using intrafascicular electrodes have not reported longer than 1 month signal stability. Thus, intrafascicular electrodes may not be a viable option for chronic neural control.

As a longer term method for obtaining peripheral nerve signals, our group has recently developed the Regenerative Peripheral Nerve Interface (RPNI). RPNIs are 2-3 cm autologous muscle grafts that are neurotized with residual severed nerves or nerve branches. The RPNIs can generate recordable high-amplitude EMG activity, acting as bioamplifiers for efferent peripheral nerve signals [23], [24]. We previously implanted RPNIs and intramuscular bipolar electrodes within two rhesus macaques, and reported the long-term safety and performance of RPNIs during a finger-level behavioral task [25]. That study demonstrated that RPNIs can be used as a control signal source for discrete classification of simple finger movements. However, their capability for continuous estimation of finger movements has yet to be quantified.

Here, we build on this prior work by pursuing continuous fingertip control using indwelling bipolar intramuscular EMG electrodes [26]. We record from both implanted RPNIs and intact muscles within two rhesus macaques. Using these signals, we evaluated the ability to control finger flexion and extension in a continuous fashion using the best-known approach from brain controlled prostheses [27], [28], the Kalman filter, as well as a Wiener filter for comparison. Recorded EMG signals were used to train these algorithms to control a virtual hand both offline and in real-time. This is the first demonstration of chronic indwelling intramuscular electrodes being used for continuous position control of fingers, and the first use of a Kalman filter with EMG from RPNIs.

II. Methods

All procedures were approved by the University of Michigan Institutional Animal Care and Use Committee. The two animals used in this study were the same two animals used in Irwin *et al.* [25].

A. System Design

RPNIs are neurotized free autologous muscle grafts that convert signals from transected residual peripheral nerves into high amplitude EMG signals [23]. The EMG signals can then be recorded from intramuscular electrodes implanted into the belly of the muscle graft. Here, two surgeries were performed to implant all RPNIs and bipolar electrodes (IM-MES, Ardiem Medical). The first surgery consisted of implanting the majority of RPNIs. Typically, RPNIs takes 3-4 months to mature and reinnervate. Here, a whole year passed before implanting the IM-MES electrodes to assess health and safety of the

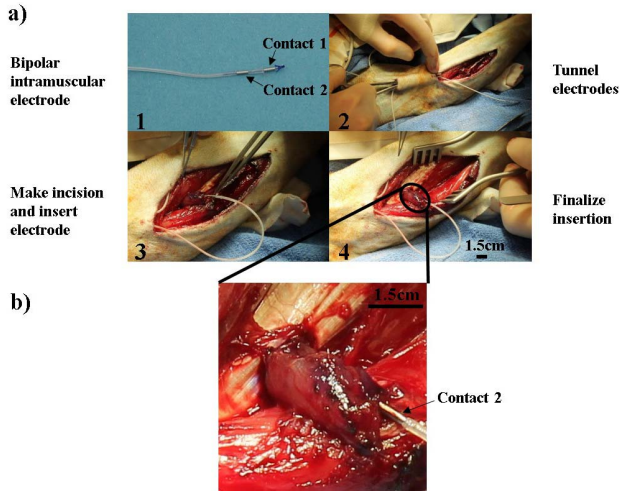

Fig. 1. (a) Bipolar electrode implantation procedure illustrated from *left* to *right*. *(1)* Representation of an IM-MES bipolar electrode (Ardiem Medical http://www.ardiemmedical.com). *(2)* Electrodes are first tunneled through the skin until reaching the site of electrode insertion. *(3)* An incision is made in the belly of the RPNI graft or muscle of interest and the electrode is inserted. *(4)* Electrode insertion is complete and the remaining slack of the electrode wire is carefully tucked in between the intact muscles to minimize electrode shift. (b) A close up of a RPNI implanted with a bipolar intramuscular electrode.

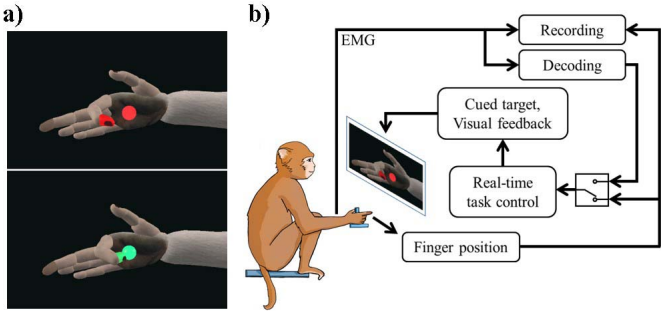

Fig. 2. Monkey behavioral task. (a) The monkey hits virtual targets by moving his four fingers simultaneously. The index finger of the virtual hand moved in conjunction with the monkey's movements. (b) The virtual hand could be controlled either by the monkey's movements directly (as measured by flex sensors) or by EMG signals decoded into movement predictions in real-time, allowing either open-loop or closed-loop task performance [22] [16]. The "decoding" and "recording" blocks in parallel indicate that recorded EMG is both stored and sent to the decoding algorithm simultaneously, giving us the ability to flip between open-loop or closed-loop control instantly.

RPNIs [25]. RPNI implantation takes ∼2-4 hours, while the IM-MES implantation takes ∼1-3 hours. A total of 9 RPNIs were implanted on separate branches of the median and radial nerves in the forearm of two rhesus macaques L and R. RPNI construction starts with harvesting a 1 x 3 cm muscle graft from a healthy native donor muscle. Then, the distal end of a targeted peripheral nerve is isolated and dissected into individual fascicles or branches. The end of the isolated nerve is sutured to the center of the muscle graft and then the muscle graft is wrapped around the nerve and sutured shut to create an enclosed housing. This procedure is repeated as needed to create the desired number of RPNIs. For our purposes, the median and radial nerve branches of interest terminated on the extrinsic finger flexors and extensors in order to gain hand level control. We used only minor, redundant terminal motor nerve branches to preserve motor function. Specifically, the median nerve branches that controlled the flexion of digits 2-5 and 1-3, and the radial nerve branch that controlled the extension of digits 2-5. Further details of the RPNI graft construction and implantation can be seen in Irwin *et al.* [25].

B. Study Design and Device Validation

Post RPNI construction, we implanted IM-MES electrodes into RPNIs neurotized by nerves which originally innervated the flexor digitorum superficialis (FDS), flexor digitorum profundus (FDP), and extensor digitorum communis (EDC) muscles. We also implanted an IM-MES electrode into an intact extensor carpi radialis (ECR) muscle in monkey L as a control. For the remaining sections below, the RPNIs will be referred to by the muscle that was originally innervated by the transplanted nerve branch, i.e. FDS RPNI. Fig. 1(a) demonstrates the electrode implantation process. These electrodes consist of two insulated stainless steel leads coiled in a double helix formation and potted in silicone tubing [26]. Contacts are formed by exposing the leads and wrapping them around the tubing, and a polypropylene anchor at the distal end secures the electrode in the muscle. In the first animal, the two contacts on the electrode were 4 mm long with a diameter of 1.27 mm (the diameter of the silicone tubing), and were separated by 6 mm. After noting that in some cases, this was too large to fit both contacts within the muscle belly of an RPNI, a reduced contact size of 1.5 mm and inter-contact spacing of 2.5 mm was used for the second animal. A single IM-MES electrode was placed in the muscle belly of each RPNI, as well as in a healthy control muscle, by making a small incision and manually feeding the electrode anchor-first into the muscle. Leads were tunneled subcutaneously to a transcutaneous port on the animal's back and attached to a connector protected by a primate jacket. A fully-implanted RPNI is shown in Fig. 1(b).

C. Behavioral Task

We trained both monkeys to perform a finger movement task, illustrated in Fig. 2. A flex sensor (Spectra Symbol) was attached to the monkey's index finger, which fed finger position data to a real-time computer running xPC Target (Mathworks). Musculoskeletal Modeling Software (MSMS; [29]) provided a virtual model of a monkey hand that was displayed in front of the monkey on a monitor, and mirrored the finger movements measured by the flex sensor. The xPC Target real-time system executes on a millisecond basis. Neural signals are collected at 30 ksps and are sent to the xPC Target via an Ethernet cable. Using a 1 Gbps Ethernet network card, data transmission time from the Cerebus to the xPC Target is trivial. Thus, the xPC Target collects 30 samples of neural data in 1 millisecond. The Kalman filter decoding algorithm can be manually set to update at arbitrary intervals. Here, we set the decoding algorithm to update every 50 ms or 100 ms. Updated position values are then sent from the xPC Target to the MSMS virtual software over Ethernet. Again, transmission

time from xPC Target to MSMS was unmeasured, but likely very small since it has very little software running. Using a 120 Hz monitor adds 8 ms.

The monkeys both performed movements with all four fingers simultaneously, with the position of all four indicated by the index flex sensor. Both monkeys L and R were trained with the virtual hand displaying only the index finger moving because this animation was the most robust and easiest to view during their earliest training sessions. However, the animal always moved all four fingers together, and all results that are present are for all four fingers moving simultaneously. Images and videos are shown below in the way they were originally viewed by the animal. At the start of a trial, the xPC cued a spherical target to appear in the path of the virtual finger. The monkey was then required to move his fingers in order to hit the target on the screen. After holding the virtual finger in the target for a required hold time (usually set to 500-700 ms), the monkey was given a juice reward. Both monkeys performed a center out task with 50% flexion denoted as center. The xPC then chose randomly between 6 targets, 3 flexion and 3 extension targets, to display next after each center target was hit. The virtual hand could also be controlled by decoding the RPNI signals in real-time into predicted movement. As described below, the monkey would receive a reward only if the predicted movement was correct, and could act to correct the decode within the trial time limit in a closed-loop manner.

D. Electrophysiology Recording

During task performance, EMG signals from the RPNIs were input into either a DAM50 differential EMG amplifier (WPI), which filtered the signal between 10-1000 Hz with a gain of 1000x, or directly into a Cerebus neural signal processor (Blackrock Microsystems), which filtered the signal between .3-7000 Hz (unity gain). For real-time signal analysis, the Cerebus was used to record from multiple electrodes simultaneously. The DAM50 was used for lower-noise recordings from a single electrode. In both cases, the processed signal was digitized and saved to disk by the Cerebus at 30 ksps. The signal was further sent from the Cerebus to the behavioral rig via ethernet, where it could be processed in real-time.

E. Signal Analysis and Decoding

To isolate the EMG signal from motion and electrical artifacts, we filtered the data between 100-500 Hz using a second-order Butterworth filter. In offline analysis, the data were filtered forwards and backwards in order to eliminate phase shift.

To assess the EMG signal quality, we calculated both the maximum voluntary contraction (MVC) and the signal to noise ratio (SNR) for each recorded RPNI and intact muscle. MVC was calculated by isolating periods of maximum agonist behavior, corresponding to either full finger flexion or full finger extension movements, depending on the function of the RPNI nerve. Approximately 1000-1400 trials were conducted within each recording session. Movement periods were isolated and labeled by thresholding the finger position and velocity to ensure both maximum EMG activation and consistent behavior. The mean of the peak-to-peak amplitude during all such movements was taken as the MVC. SNR was calculated by simply dividing the MVC by the noise floor of the channel, which was extracted by manually selecting around 60-130 second quiescent periods in the signal and calculating the mean peak-to-peak amplitude.

To evaluate the stability of the IM-MES electrode over time, we measured the amplitude of recorded single motor unit activity from the EMG. Single unit activity was extracted manually by choosing the peak of the motor unit waveform during behavior segments where finger position remained constant and finger velocity was approximately zero. Two milliseconds of samples were taken before the peak and 6 ms after the peak. 100 examples of one motor unit were extracted per recording session approximately once a week, and the mean and variance of the motor unit amplitude were calculated. Each motor unit was chosen based on having the same shape. If the signal was perfectly stable, the amplitude of the motor unit would remain the same over time. Thus, by picking the same motor unit over time, we attempted to assess the variability of the recorded EMG signal and the stability of the IM-MES electrodes.

To assess the functional efficacy of the recorded RPNI signals, we used a Kalman filter to decode continuous finger position movements from the EMG signals. The Kalman filter is a recursive linear filter that tracks the state of a dynamical system throughout time using noisy measurements [27], [28], [30] relying on a trajectory model and an observation model. Here, the trajectory model is a representation of the transition of the kinematic state of the fingers at time t to time $t+1$. We assume that the finger state vector x_t represents the position and velocity of the finger,

$$x_t = \left[pos_{t,} vel_t, 1\right]^T \tag{1}$$

where pos_t is the finger position measured by the bend sensor and vel_t is the calculated difference of the position. The observation model represents the noisy transformation of the current finger state to recorded neural activity. Here, temporal characteristics of the EMG waveform represented the neural activity. We extracted two temporal characteristic features of the EMG waveform: (1) mean absolute value (MAV) and (2) waveform line length (LL) [31], [32]. Mean finger kinematics and EMG features were computed in consecutive time bins. Decoding features were extracted from the flexor and extensor channel available for both monkeys. A total of two channels were input into the filter during offline and online analysis. In particular, these features were simultaneously obtained from the FDP and EDC RPNI in monkey L and the FDS RPNI and an intact extensor muscle in monkey R. For monkey R only the MAV was used as a feature. If we let $\vec{y}_t = [y_1 ..., y_k]^T$, where y_k is the temporal feature of the kth electrode, then the linear relationship between the finger state and neural measurements is:

$$\vec{x}_t = A\vec{x}_{t-1} + \vec{w}_t \tag{2}$$

$$\vec{y}_t = C\vec{x}_t + \vec{q}_t \tag{3}$$

where $A \in \boldsymbol{R}^{3\ x3}$ and $C \in \boldsymbol{R}^{kx3}$ represent the trajectory and observation models, and $\vec{w}_t$ and $\vec{q}_t$ are Gaussian distributed

noise terms for the state trajectory transition and the observation transformation, respectively. A is the linear transformation from the previous finger state to the current finger state (the trajectory model), while C is a mapping of the current finger state to the EMG temporal features (the observation model).

The above analysis was done both offline and in online closed-loop sessions. During closed-loop sessions, both monkeys performed a center-out task. After ~200 trials of normal task performance, the decoder was trained and the virtual hand was switched to mirror the Kalman filter output (predicted position values) instead of the flex sensor output. The Kalman filter updated every 50 ms, or 100 ms on some online sessions, allowing continuous control of the virtual hand.

For comparison in performance, a Wiener filter was also implemented both offline and online for monkey R and only offline for monkey L. A comparable study used Wiener filters as a baseline comparison for decoding performance between different algorithms [18]. The Wiener filter equation is as follows:

$$\vec{x}_t = B\vec{y}_t + \vec{b}_0 \tag{4}$$

where $\vec{x}_t$ represents the kinematic state of the system and $\vec{y}_t$ is the featured neural activity, where $\vec{y}_t$ equals $[y_1, y_2, ..., y_k]^T$, representing a history of measurements up to time k.B is the linear transformation of the neural features to the kinematic state and $\vec{b}_0$ is a constant offset.

For offline performance evaluation, tenfold cross validation was implemented when training the Kalman filter and Wiener filter. Subsequently, accuracy of the reconstructed position trajectory was calculated via cross-correlation (CC) with the actual trajectory. Likewise, root mean squared error (RMSE) was calculated between the reconstructed and actual trajectories. Let $\hat{x}_t$ be the estimate for the true position x_t, then the CC and RMSE are defined as follows:

$$CC = \frac{\sum_t (x_t - \bar{x}_t)(\hat{x}_t - \bar{\hat{x}}_t)}{\sqrt{\sum_t (x_t - \bar{x}_t)^2 \sum_t (\hat{x}_t - \bar{\hat{x}}_t)^2}} \tag{5}$$

$$RMSE = \sqrt{\frac{1}{T}\sum_{t=1}^{T} \left(x_t - \hat{x}_t\right)^2} \tag{6}$$

where $\bar{x}_t$ represents the mean of the x position, $\bar{\hat{x}}_t$ represents the mean of the estimated position, and T represents the sample size of the predicted and actual position measurement.

For real-time performance metrics, we calculated throughput, described by Fitts's law [33], [34], and average success percentage. Fitts's law, which calculates an overall bit rate, has been shown to be a robust performance metric for continuous brain machine interfaces (BMIs) across different task parameters. The Fitts's equation used is shown below.

$$Throughput = \frac{\log_2\left(1 + \frac{D}{W}\right)}{Movement\ time}\ (bits\ per\ second) \tag{7}$$

Here, D is the distance between targets and W the width of the target. In addition to performance, we evaluated the smoothness of the estimated path trajectory between targets. In both offline and online analysis, the jitter metric was calculated by counting the number of times the velocity of the estimated trace changed signs and normalizing that number to the total experiment time to obtain the number of sign changes (SC) per second.

To gauge the limits of recalibrating the decoding algorithms between recording sessions, Wiener filter parameters were trained offline on an initial EMG recording day and reused for decoding with subsequent EMG recording days. CC and RMSE values were calculated for each day to measure the performance. As a baseline for comparison, new Wiener filter parameters were trained on each day, used to decode that day's EMG, and CC and RMSE values were calculated.

Overall for decoding analysis, a total of 7 recording session datasets were used for offline and online analysis between both monkeys. For signal stability measures and further functional efficacy, 12 datasets were used over the span of 8 weeks to extract single units and train the Wiener filter parameters. Unless otherwise stated, paired t-tests were used to evaluate the differences in CC and RMSE measurements between the decoding filters within each monkey (n = 2). Additionally, unpaired t-tests were used to evaluate the differences of single unit waveform amplitude between days.

III. Results

A. Signal Quality Over Time From Indwelling Electrodes

A total of 8 muscles were recorded with indwelling electrodes, 4 in each monkey. For monkey L, the FDP and EDC RPNI were used for offline and online continuous decoding analysis, as they provided task-relevant finger flexion and extension information. The intact ECR was not used since it only contained wrist information. Additionally, due to connector breakage, the FDS RPNI did not show finger flexion information during online continuous decoding. However, the FDS RPNI signal did appear during previously-reported online discrete decoding using a percutaneous electrode [25]. For monkey R, the FDS RPNI and intact EDC were used for decoding. The IM-MES electrode in the intact EDC was originally placed in the EDC RPNI, but high amplitude was immediately recorded after implantation, which could not have been produced by a denervated muscle. Thus, the electrode was assumed to have slipped out of the RPNI and was recording from surrounding EDC muscle. Similar to monkey L, the FDP RPNI channel was not used due to connector breakage.

For both monkeys, the maximum voluntary contraction (MVC) and signal to noise ratio (SNR) of the EMG signals used for decoding are shown in table 1. Here it is important to note that each RPNI muscle graft surrounds a single small branch of the median and radial nerves, with an IM-MES electrode inside that graft. Consistent with this, the RPNI signals had an average SNR of 7.92, smaller than the intact EDC muscle with an SNR of 39.8 but greater than the SNRs reported for intrafascicular electrodes [19], [22]. Fig. 3 shows the intramuscular raw EMG signals from both flexor and extensor RPNIs and intact EDC, bandpass filtered from 100-500 Hz. The top row represents each monkey's finger movements during the behavioral task (as a percentage of fully-flexed, with zero as fully-extended).

TABLE I
MAXIMUM VOLUNTARY CONTRACTION AND SIGNAL-TO-NOISE OF IMPLANTED ELECTRODES

Monkey	Muscle	MVC (μV)	SNR
L	FDP RPNI	103.9	7.42
	EDC RPNI	136.2	9.77
R	FDS RPNI	19.59	6.58
	Intact EDC	936.2	39.8

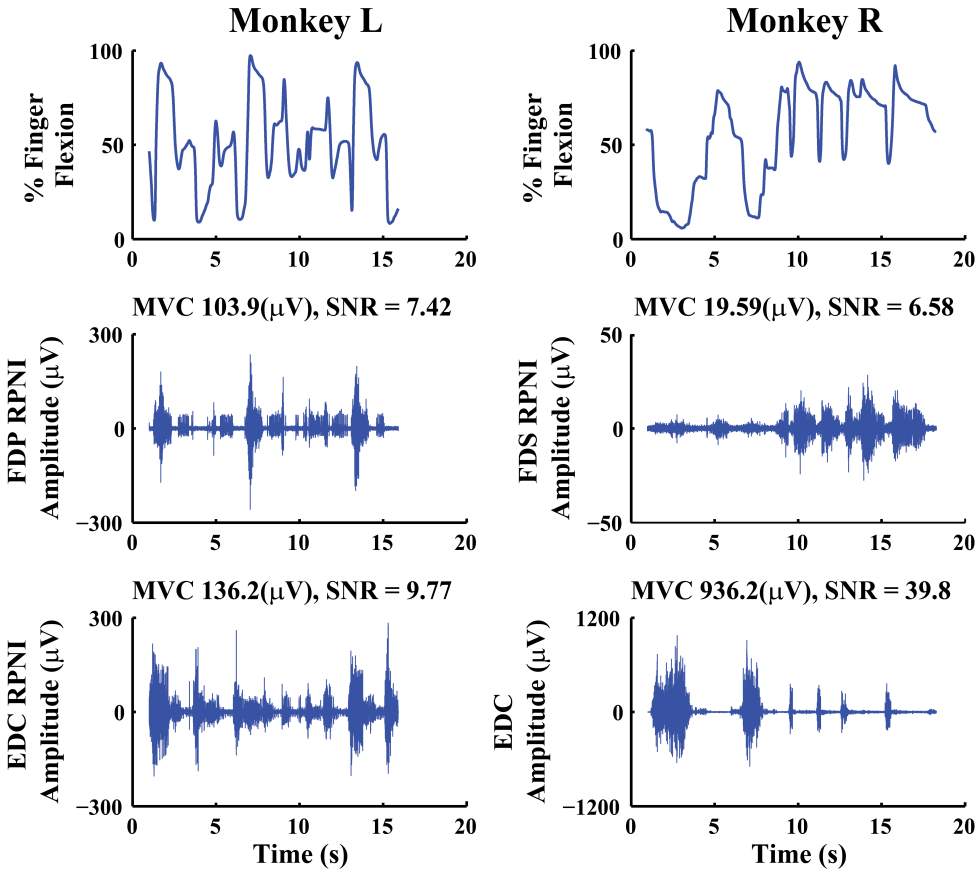

Fig. 3. Example of recorded EMG from chronic IM-MES electrodes in both monkeys. The *top* trace in each column is finger position during task behavior. The *bottom* two rows in the *left* column are the EMG signals from the flexor and extensor RPNIs in monkey L. The *bottom* two rows in the *right* column are the EMG signals from the flexor RPNI and the intact EDC in monkey R. The displayed raw signals came from online continuous finger control recording sessions, which differ from the signals reported in Irwin *et al.* [22], [16].

B. Offline Continuous Reconstruction

Using the Kalman filter, which uses only the past 50 ms bin for input, there was an overall average CC of 0.89 and 0.84, and RMSE of 0.112 and 0.140, for monkey L and R respectively. This performance is similar to another study using a linear regression algorithm with intramuscular EMG during an annulus target task [35]. Overall, the Kalman filter had smooth transitions between targets but would occasionally overshoot near the minimum and maximum finger positions. This may be a result of un-modeled non-linearities in the relationship between EMG and finger position.

To compare performance with the Kalman filter, we applied the Wiener filter to the same training and testing datasets. Fig. 4 illustrates the reconstruction of true position offline using both Kalman and Wiener filters in monkeys L and R. Wiener filters have been used both offline and online in cortical brain machine interfaces (BMIs) for linear reconstruction [28]. Additionally, Smith *et al.* [18], [35] has used the Wiener filter as a baseline comparison to their algorithm's performance with intramuscular EMG. Here, the Wiener filter had an overall average CC of 0.91 and 0.83 and RMSE of 0.0883 and 0.121, for monkey L and R respectively.

Although this performance was not significantly different than the Kalman filter ($p = 0.643$), it was dependent on 500 ms of past EMG signal (10 bins). Without history, the overall average CC was 0.66 and 0.68 with an RMSE of 0.157 and 0.161 for monkey L and R respectively. This is a significant drop compared to the Kalman filter ($p < 0.001$). Additionally, the Kalman filter was smoother than the Wiener filter with or without history, with an average jitter of 1.7 and 1.4 in monkeys L and R, respectively, compared to 2.3 and

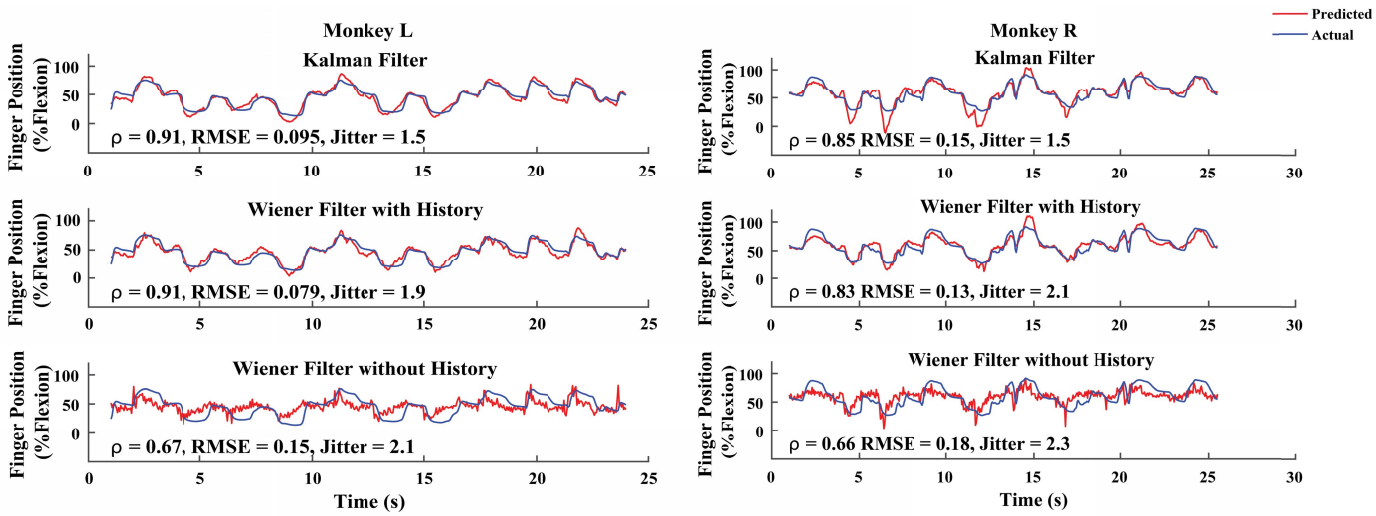

Fig. 4. Offline continuous reconstruction. Traces were produced from one of the recording sessions from each monkey. CC, RMSE, and Jitter values are mean values for each filter across datasets. The top traces in each column are the offline predicted reconstructions (red) overlapping on the actual finger position (blue) for the Kalman filter. Middle traces illustrate the same reconstructions for the Wiener filter with 500ms of history and the bottom traces show the reconstruction for the Wiener filter without history (using a single 50 ms bin).

TABLE II
OFFLINE DECODING PERFORMANCE METRICS FOR MONKEYS L AND R

		Kalman Filter			Wiener Filter with History			Wiener Filter without History		
Monkey	Session	CC	RMSE	Jitter (#SC/s)	CC	RMSE	Jitter (#SC/s)	CC	RMSE	Jitter (#SC/s)
L	1	0.88	0.12	1.6	0.92	0.083	2.2	0.64	0.17	2.0
	2	0.89	0.10	1.7	0.90	0.082	2.4	0.64	0.15	1.8
	3	0.91	0.095	1.5	0.91	0.079	1.9	0.67	0.15	2.1
	4	0.87	0.14	1.9	0.89	0.11	2.5	0.69	0.17	2.8
	Mean	0.89	0.11	1.7	0.91	0.088	2.3	0.66	0.16	2.2
R	1	0.85	0.15	1.5	0.83	0.13	2.1	0.66	0.18	2.3
	2	0.84	0.13	1.3	0.85	0.11	1.7	0.70	0.15	2.0
	3	0.82	0.14	1.5	0.83	0.11	1.9	0.68	0.15	1.8
	Mean	0.84	0.14	1.4	0.83	0.12	1.9	0.68	0.16	2.1
Overall	Mean	0.87	0.12	1.6	0.88	0.10	2.1	0.67	0.16	2.1

1.9 for the Wiener filter (2.2 and 2.1 for the Wiener filter without history).

Table II shows the performance metrics for all sessions conducted with monkeys L and R. The Wiener filter with and without history had significantly higher jitter than the Kalman filter ($p < 0.01$). This is expected due to the Kalman filter's trajectory model, which is based on a physics model of the kinematics of the finger. Thus, although the performance of the Wiener filter can be equal to that of the Kalman filter, it requires history. Other studies have previously shown that adding neural data from hundreds of milliseconds in the past can significantly lower performance [36].

C. Online Continuous Control

During online control sessions, both monkeys performed the center-out task in hand control (controlled by flex sensor) and neural control (controlled by EMG signals) form. A summary of the overall average success rate, average acquisition time, and throughput for Kalman and Weiner filters can be seen in tables 3 and 4. For monkey L, the Kalman filter in session 1 used 50ms bins of neural data, while session 2 used 100 ms bins. The target could randomly appear in 6 different locations, 3 flexion and 3 extension targets after the center target was hit. Animals had to hold their hand within the acquired target space for 500- 700ms to receive the reward. Fig. 5 shows a sample of the online neural control task performance with the Kalman filter for both monkeys and the Wiener filter for monkey R. Both the estimated finger position and the actual finger position are displayed over time.

For a comparison baseline, the animals had an overall average success rate of 98.50% using hand control, and an average time to target of 1.25 sec. The animals were able to acquire targets with a high success rate using an online Kalman filter, albeit at a slower pace with a significant difference between the time to success compared to hand control ($p < 0.001$). Specifically, their overall success rate was 96.70% with an average time to target of 1.61 sec. This was 77.64% as fast as hand control. The overall throughput was 0.77 bits/s, which was 93.90% of the throughput under hand

TABLE III
ONLINE KALMAN FILTER TASK PERFORMANCE METRICS FOR MONKEYS L AND R

		Success (%)		Mean Time to Success (s)		Throughput (bits/s)		Jitter (# SC/s)
Monkey	Session	Hand Control	Neural Control	Hand Control	Neural Control	Hand Control	Neural Control	Neural Control
L	1	100	96.3	1.21	1.66	0.79	0.68	3.5
	2	94.3	94.9	1.31	1.77	0.71	0.66	4.7
	Mean	97.1	95.6	1.26	1.72	0.75	0.67	4.1
R	1	100	99.4	1.23	1.49	0.86	0.85	2.6
	2	99.9	97.0	1.24	1.50	0.92	0.88	3.2
	3	99.7	97.0	1.22	1.48	0.87	0.85	3.7
	Mean	99.9	97.8	1.23	1.49	0.88	0.86	3.2
Overall	Mean	98.5	96.7	1.25	1.61	0.82	0.77	3.6

TABLE IV
ONLINE WIENER FILTER TASK PERFORMANCE METRICS FOR MONKEY R

		Success (%)		Mean Time to Success (s)		Throughput (bits/s)		Jitter (# SC/s)
Monkey	Session	Hand Control	Neural Control	Hand Control	Neural Control	Hand Control	Neural Control	Neural Control
W	1	97.48	92.58	1.27	1.99	0.95	0.68	4.4
	2	99.55	98.20	1.14	1.68	0.96	0.69	4.7
	Mean	98.52	95.39	1.21	1.84	0.96	0.69	4.5

control. See supplemental video 1 for a video of online, neural control of the virtual hand using the Kalman filter.

For one animal, the Wiener filter with history was also used online, and resulted in a statistically significant smaller average throughput of 0.69 bits/s, 79.65% of the throughput under Kalman filter control ($p < 0.001$). The average success rate and acquisition time were not statistically different ($p = 0.55$, 0.27, respectively). However, on average the acquisition time for the Wiener filter was longer than the Kalman filter, 1.84 to 1.49 sec, even though statistical significance was not met. This would tend to lower the Wiener filter's throughput average, suggesting that the 500ms history did have some negative impact on the performance. See supplemental video 2 for a video of online, neural control of the virtual hand using the Wiener filter. Finally, similar to the cursor jitter measured offline, we found a significant difference between the Kalman filter and Wiener filter online in monkey R ($p = 0.043$). This suggests that orbiting behaviors may have played a role in longer target acquisition time, which resulted in lower throughput. For monkey L, only the online Kalman filter was implemented.

D. Recalibration Longevity

Surface EMG is the standard control signal used in clinical myoelectric prostheses. However, surface EMG electrodes myoelectric prostheses. However, surface EMG electrodes have some limitations that contribute to the rejection of myoelectric prosthetic use. Surface electrodes can shift on the skin, which can cause EMG instability [56]. Additionally, perspiration can alter the electrical impedance of the electrode such that the system's performance reduces [51]. This reduction in functionality can cost time for the user and add frustration to the usage of the prosthetic. Thus, a system where the EMG signal remains stable would be desirable.

To assess the functional stability of the intramuscular EMG over time, the FDP and FDS RPNIs in monkey L were fed individually into a Wiener filter offline. This was done because the EDC RPNI was created at the same time as the IM-MES electrodes were implanted. Thus, a waiting period was required to allow the EDC RPNI to fully mature to produce EMG activity. Since the Kalman filter required both the extensor and flexor RPNI inputs to function, this prevented full evaluation of the recalibration longevity measurement. As an alternative, we used the Wiener filter to test the functional stability of individual flexor RPNIs.

The Wiener filter decoder parameters were trained on an initial EMG recording day and reused on subsequent EMG recording days. As a comparison, decoding parameters were also recalibrated on the same days and CC and RMSE values were measured for both conditions (uncalibrated vs. recalibrated). Fig. 6a illustrates the performance of each RPNI, showing the change of CC and RMSE values over time (blue line). The red line indicates measured performance based on recalibrated decode parameters.

For the FDP RPNI, CC values of the uncalibrated decoder were slightly lower compared to the calibrated decoder's CC values for each day. Contrarily, the FDS RPNI did not have a significant change in CC values between uncalibrated and calibrated decoders ($p = 0.165$). While correlation coefficients are not sensitive to large changes in amplitude, this result suggests that the timing of decoded flexion and extension was consistent across days without recalibration. While the signals may provide some form of stable functionality over

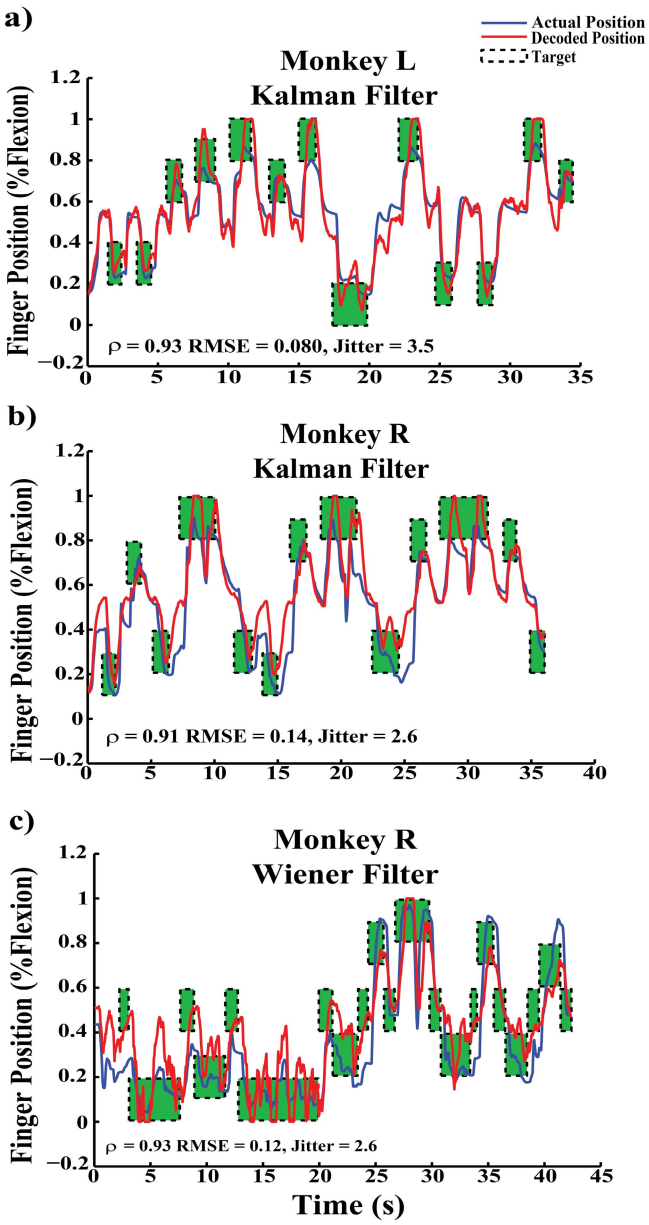

Fig. 5. Online continuous control. (a), (b) Traces in each row are the online predictions (red) overlapping on the actual finger positions (blue) for the Kalman filter in monkey L (a) and the Kalman and Wiener filter with history in monkey R (b), (c), respectively. Each trace also displays the target area, where height of the area represents the size of the virtual target, while the width of the area represents how long the virtual target was displayed. Green target areas denotes a successful target hit.

time, they may also cause an undesired overshoot at the minimum and maximum finger positions. To investigate this further, the RMSE showed clear visible changes over time. Both the FDP and FDS had significant difference between RMSE values ($p < 0.05$).

Looking more closely at the data, there was an increase in error centered on day 79. Average single units from the FDP RPNI are shown across time throughout this period (Fig. 6b). 100 examples of a chosen motor unit during consistent near zero velocity and constant position behavior were extracted from the FDP RPNI. The extracted single unit's amplitude changed by a maximum factor of +18.65% and a minimum factor of −25.85% compared to its mean over the recorded time period, which was a significant change ($p < 0.05$). While we do not know for certain that this was the same unit, the changes correspond well to increased errors in the decode, with day 79 showing the most significant change. Overall, this suggests that intramuscular EMG signal amplitude varies over time, which may be due to either RPNIs still maturing 16+ months post-implantation, or the IM-MES electrodes shifting during the monkey's non-task related free time. This varying amplitude would not be desired in a practical myoelectric control system.

IV. Discussion

In this study, we demonstrated continuous control of finger position using intramuscular EMG electrodes in RPNIs using a Kalman filter. To the best of our knowledge, this is the first demonstration of RPNI continuous control of all four finger movements using indwelling electrodes. Previous continuous decoding studies have either used percutaneous fine-wire electrodes or surface electrodes to obtain EMG signals [13], [14], [35], [38] with few decoding isolated finger movements [16], [39]. Other studies using indwelling electrodes have only implemented classifiers or proportional control algorithms [40], [41].

Overall offline, the Kalman filter had a smoother position output compared to the Wiener filter for both monkeys. Online we did not see a significant difference in the jitter between the Kalman and Wiener filter in monkey R, but qualitatively from supplemental video 2, we can see that control of the virtual hand was more difficult. This reflects the Wiener filter's significantly lower throughput compared to the Kalman filter's throughput. Thus, in a practical system, the Wiener filter with history would not provide the appropriate control for finger-level fine motor skills.

Though the Kalman filter demonstrated the ability to provide continuous finger control, there are some challenges that need to be addressed. Primarily, we limited the number of DOFs to a simple open-close to demonstrate the capabilities of RPNIs as a proof of concept. To add more movement types, more RPNIs would need to be created with separated fascicles from each nerve. Studies have shown that distinct somatotopic organization occurs within peripheral nerves [55]. For example, nerve fibers innervating a specific muscle remain grouped together throughout most of the nerve. This is promising for separating nerves into discrete functional RPNIs and then potentially recording independent signals, increasing the number of DOF control sources. Additionally, monkeys will need to be trained on a new behavioral task that encompasses different grasp movements. Future studies are needed to measure and compare performances between different grasp movements using multiple RPNIs, and the question of individuated finger movements may ultimately be easier to address in humans.

Secondly, the Kalman filter reconstruction caused overshoots during some periods of flex and extend movements. This may indicate that the assumptions of a linear relationship between EMG activity and finger kinematics are erroneous.

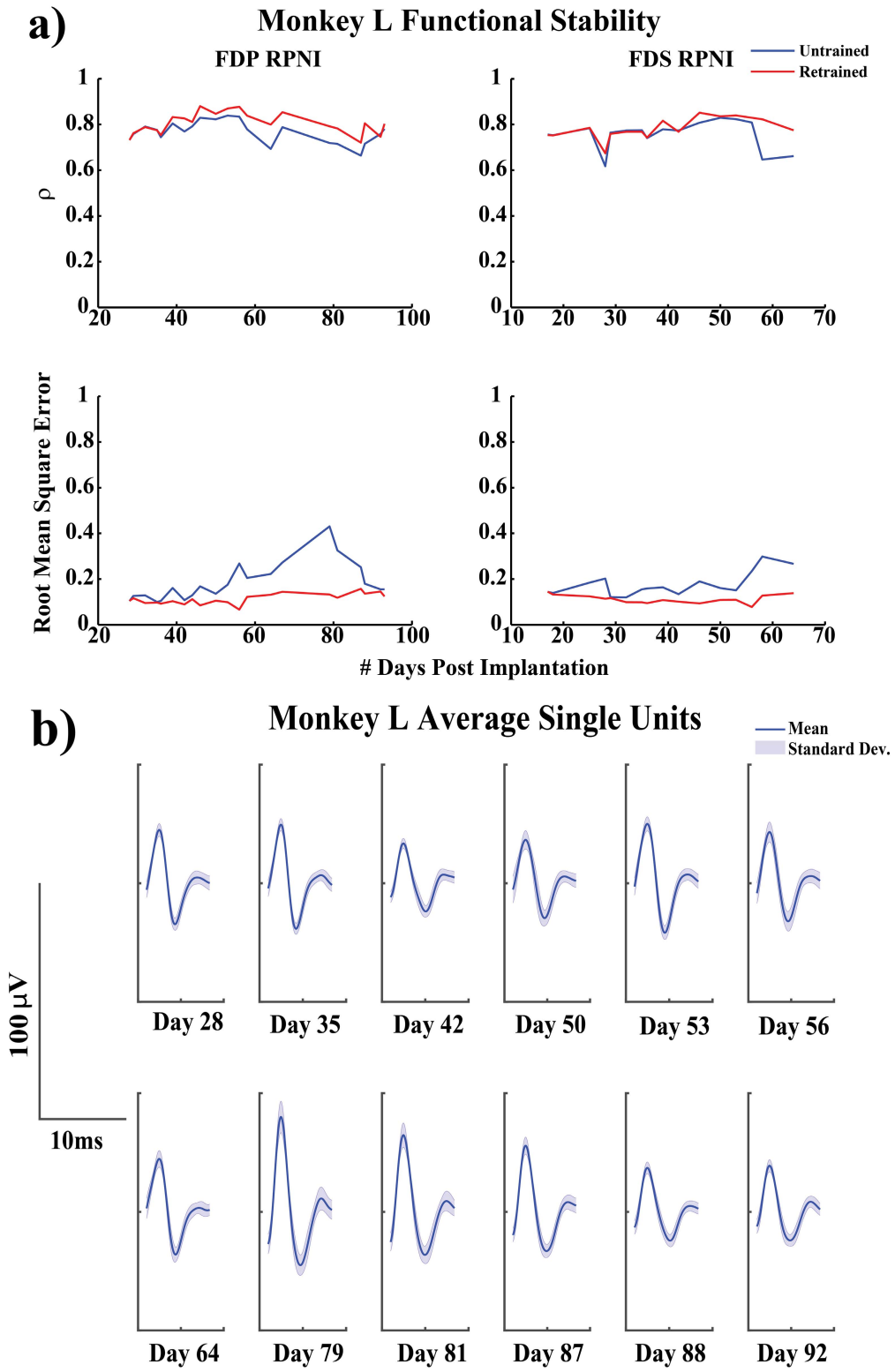

Fig. 6. Functional stability and single unit activity. (a) Decoding parameters were trained on Day 28 for monkey L and reused to decode finger position on subsequent days. In (a) blue line denotes the decoding performance for the FDP and FDS RPNI over time for uncalibrated decoder parameters. Red line indicates decoding performance over time after recalibration. (b) 100 examples of one motor unit were extracted and averaged once a week for 8 weeks.

Nonlinear methods such as artificial neural networks, support vector regression, and kernel-ridge regression have been evaluated using surface EMG [13], [15], [16], [38] but no physiological model of the EMG to kinematic states has been used for prosthetic control. The results from [16] show that a Gaussian process regression had an average correlation

coefficient of 0.84 using 8 surface electrodes. For a single DOF, their best estimate for the MCP, PIP, and DIP joints were 0.92, 0.85, and 0.79, respectively. Comparatively, the Kalman filter for a single DOF performs just as well as this decoder with 2 intramuscular bipolar electrodes. Although RPNIs may not offer higher regression accuracy, they are able to produce relevant EMG signals from peripheral nerves, which could ultimately lead to many more independent EMG signals associated with missing or deep musculature, unlike surface EMG. The small number of nonlinear studies may be attributed to the recent interest of muscle synergies and how muscle activity during movement can be broken down into linear combinations [42]. However, muscle synergies may not be as important in intramuscular EMG because of the single motor unit activity that can be picked up from intramuscular electrodes. Most studies have used Hill-based muscle models or other biomechanical models to predict forces of one or two DOFs [49], [50], [53]. These studies have reported high motor performance, demonstrating that nonlinear algorithms could provide a better solution to current clinical control algorithms. Thus, more exploration is needed to investigate potential nonlinear relationships that may exist between intramuscular EMG and finger kinematics.

Furthermore, we investigated the recalibration longevity in order to assess the stability of intramuscular EMG. Surface EMG has numerous limitations, discussed earlier, which prevent it from being an ideal solution to myoelectric prosthesis control. In this study, we purposefully used only electrodes with a strong existing safety record in humans [26], to enable fast translation. These bipolar electrodes had large contact sizes and low impedance, but were limited to a small number of channels due to the wiring. To investigate cross-talk issues, one bipolar electrode was implanted into an intact extensor carpi radialis (ECR) muscle as a control. Signals compared between the EDC RPNI and intact ECR muscle showed different amplitudes and shape. Additionally, the EDC RPNI fired more frequently during the behavioral movements than the ECR. Thus, any existence of cross-talk between the bipolar electrodes appeared to be minimal.

The higher SNR reported here and by others [37], [43], motivates additional development in multi-channel intramuscular EMG electrodes, as it is very likely that additional channels could provide anatomically precise information about additional joints simultaneously. For example, multi-channel intramuscular thin film electrodes have been demonstrated in both animals and humans for multi-motor unit recordings [44], [45]. Single units were generally visible on even these macroscopic electrodes, and remained high throughout 7 months of implantation in two animals. However, single unit waveforms were not identical from day to day. Quantitatively, they varied much less than Utah array waveforms [46], and there were no systematic changes indicative of progressive scarring. However, as EMG electrodes get smaller and more numerous over time, the biological environment around them may shift similar to brain electrodes. This may require adaptive approaches to stabilize the control signal [47], [48] or further investigation for different electrode designs to mitigate this effect.

Overall, these results suggest that future implantable systems may be more able to precisely control the position of individual joints. While many advanced prosthetic hands have fully articulated fingers and other joints (Touch Bionics, Deka), most are not natively capable of position-based control. Future designs may need to take the availability of these novel control signals into account, for example in making hands that can sense their current position for real time adjustment. For future studies, we would like to (1) increase the number of EMG electrodes that can be implanted simultaneously to obtain higher functionality, and (2) evaluate the use and controllability of multiple DOFs both individually and in combination. Combined with intramuscular recording of EMG, Kalman filter based positional control may provide patients with more naturalistic movements of their prosthetic limb.

REFERENCES

[1] T. R. Dillingham, L. E. Pezzin, and E. J. Mackenzie, "Limb amputation and limb deficiency: Epidemiology and recent trends in the United States," *Southern Med. J.*, vol. 95, no. 8, pp. 875–883, Aug. 2002.

[2] K. Ziegler-Graham, E. J. MacKenzie, P. L. Ephraim, T. G. Travison, and R. Brookmeyer, "Estimating the prevalence of limb loss in the United States: 2005 to 2050," *Arch. Phys. Med. Rehabil.*, vol. 89, no. 3, pp. 422–429, Mar. 2008.

[3] A. D. Roche, H. Rehbaum, D. Farina, and O. C. Aszmann, "Prosthetic myoelectric control strategies: A clinical perspective," *Current Surg. Rep.*, vol. 2, no. 3, pp. 1–11, Jan. 2014.

[4] K. Englehart, B. Hudgin, and P. A. Parker, "A wavelet-based continuous classification scheme for multifunction myoelectric control," *IEEE Trans. Biomed. Eng.*, vol. 48, no. 3, pp. 302–311, Mar. 2001.

[5] J. U. Chu, I. Moon, and M. S. Mun, "A real-time EMG pattern recognition system based on linear-nonlinear feature projection for a multifunction myoelectric hand," *IEEE Trans. Biomed. Eng.*, vol. 53, no. 11, pp. 2232–2239, Nov. 2006.

[6] G. N. Saridis and T. P. Gootee, "EMG pattern analysis and classification for a prosthetic arm," *IEEE Trans. Biomed. Eng.*, vol. BME-29, no. 6, pp. 403–412, Jun. 1982.

[7] R. N. Khushaba, S. Kodagoda, M. Takruri, and G. Dissanayake, "Toward improved control of prosthetic fingers using surface electromyogram (EMG) signals," *Expert Syst. Appl.*, vol. 39, no. 12, pp. 10731–10738, Sep. 2012.

[8] F. V. G. Tenore, A. Ramos, A. Fahmy, S. Acharya, R. Etienne-Cummings, and N. V. Thakor, "Decoding of individuated finger movements using surface electromyography," *IEEE Trans. Biomed. Eng.*, vol. 56, no. 5, pp. 1427–1434, May 2009.

[9] G. Tsenov, A. H. Zeghbib, F. Palis, N. Shoylev, and V. Mladenov, "Neural networks for online classification of hand and finger movements using surface EMG signals," in *Proc. 8th Seminar Neural Netw. Appl. Electr. Eng.*, 2006, pp. 167–171.

[10] A. B. Ajiboye and R. F. Weir, "A heuristic fuzzy logic approach to EMG pattern recognition for multifunctional prosthesis control," *IEEE Trans. Neural Syst. Rehabil. Eng.*, vol. 13, no. 3, pp. 280–291, Sep. 2005.

[11] C. Cipriani *et al.*, "Online myoelectric control of a dexterous hand prosthesis by transradial amputees," *IEEE Trans. Neural Syst. Rehabil. Eng.*, vol. 19, no. 3, pp. 260–270, Jun. 2011.

[12] T. A. Kuiken, "Targeted muscle reinnervation for real-time myoelectric control of multifunction artificial arms," *JAMA*, vol. 301, no. 6, pp. 619–628, Feb. 2009.

[13] J. M. Hahne *et al.*, "Linear and nonlinear regression techniques for simultaneous and proportional myoelectric control," *IEEE Trans. Neural Syst. Rehabil. Eng.*, vol. 22, no. 2, pp. 269–279, Mar. 2014.

[14] N. Jiang, H. Rehbaum, I. Vujaklija, B. Graimann, and D. Farina, "Intuitive, online, simultaneous, and proportional myoelectric control over two degrees-of-freedom in upper limb amputees," *IEEE Trans. Neural Syst. Rehabil. Eng.*, vol. 22, no. 3, pp. 501–510, May 2014.

[15] S. Muceli and D. Farina, "Simultaneous and proportional estimation of hand kinematics from EMG during mirrored movements at multiple degrees-of-freedom," *IEEE Trans. Neural Syst. Rehabil. Eng.*, vol. 20, no. 3, pp. 371–378, May 2012.

[16] J. G. Ngeo, T. Tamei, and T. Shibata, "Continuous and simultaneous estimation of finger kinematics using inputs from an EMG-to-muscle activation model," *J. NeuroEng. Rehabil.*, vol. 11, no. 1, p. 122, Aug. 2014.

[17] R. J. Smith, D. Huberdeau, F. Tenore, and N. V. Thakor, "Real-time myoelectric decoding of individual finger movements for a virtual target task," in *Proc. Annu. Int. Conf. IEEE Eng. Med. Biol. Soc.*, Sep. 2009, pp. 2376–2379.

[18] L. H. Smith, T. A. Kuiken, and L. J. Hargrove, "Evaluation of linear regression simultaneous myoelectric control using intramuscular EMG," *IEEE Trans. Biomed. Eng.*, vol. 63, no. 4, pp. 737–746, Apr. 2016.

[19] T. S. Davis *et al.*, "Restoring motor control and sensory feedback in people with upper extremity amputations using arrays of 96 microelectrodes implanted in the median and ulnar nerves," *J. Neural Eng.*, vol. 13, no. 3, p. 036001, 2016.

[20] G. S. Dhillon, S. M. Lawrence, D. T. Hutchinson, and K. W. Horch, "Residual function in peripheral nerve stumps of amputees: Implications for neural control of artificial limbs[1]," *J. Hand Surg.*, vol. 29, no. 4, pp. 605–615, Jul. 2004.

[21] S. Micera *et al.*, "Decoding information from neural signals recorded using intraneural electrodes: Toward the development of a neurocontrolled hand prosthesis," *Proc. IEEE*, vol. 98, no. 3, pp. 407–417, Mar. 2010.

[22] P. M. Rossini *et al.*, "Double nerve intraneural interface implant on a human amputee for robotic hand control," *Clin. Neurophysiol.*, vol. 121, no. 5, pp. 777–783, May 2010.

[23] T. A. Kung, N. B. Langhals, D. C. Martin, P. J. Johnson, P. S. Cederna, and M. G. Urbanchek, "Regenerative peripheral nerve interface viability and signal transduction with an implanted electrode," *Plastic Reconstruct. Surg.*, vol. 133, no. 6, pp. 1380–1394, Jun. 2014.

[24] D. C. Ursu, M. G. Urbanchek, A. Nedic, P. S. Cederna, and R. B. Gillespie, "*In vivo* characterization of regenerative peripheral nerve interface function," *J. Neural Eng.*, vol. 13, no. 2, p. 026012, 2016.

[25] Z. T. Irwin *et al.*, "Chronic recording of hand prosthesis control signals via a regenerative peripheral nerve interface in a rhesus macaque," *J. Neural Eng.*, vol. 13, no. 4, p. 046007, 2016.

[26] W. D. Memberg, T. G. Stage, and R. F. Kirsch, "A fully implanted intramuscular bipolar myoelectric signal recording electrode," *Neuromodulation Technol. Neural Interface*, vol. 17, no. 8, pp. 794–799, Dec. 2014.

[27] S.-P. Kim, J. D. Simeral, L. R. Hochberg, J. P. Donoghue, and M. J. Black, "Neural control of computer cursor velocity by decoding motor cortical spiking activity in humans with tetraplegia," *J. Neural Eng.*, vol. 5, no. 4, p. 455, 2008.

[28] W. Wu, Y. Gao, E. Bienenstock, J. Donoghue, and M. Black, "Bayesian population decoding of motor cortical activity using a Kalman filter," *Neural Comput.*, vol. 18, no. 1, pp. 80–118, Jan. 2006.

[29] M. Hauschild, R. Davoodi, and G. E. Loeb, "A virtual reality environment for designing and fitting neural prosthetic limbs," *IEEE Trans. Neural Syst. Rehabil. Eng.*, vol. 15, no. 1, pp. 9–15, Mar. 2007.

[30] R. E. Kalman, "A new approach to linear filtering and prediction problems," *Trans. ASME, D, J. Basic Eng.*, vol. 82, pp. 35–45, 1960.

[31] B. Hudgins, P. Parker, and R. N. Scott, "A new strategy for multifunction myoelectric control," *IEEE Trans. Biomed. Eng.*, vol. 40, no. 1, pp. 82–94, Jan. 1993.

[32] P. Zhou *et al.*, "Decoding a new neural–machine interface for control of artificial limbs," *J. Neurophysiol.*, vol. 98, no. 5, pp. 2974–2982, Nov. 2007.

[33] R. W. Soukoreff and I. S. MacKenzie, "Towards a standard for pointing device evaluation, perspectives on 27 years of Fitts' law research in HCI," *Int. J. Hum.-Comput. Stud.*, vol. 61, no. 6, pp. 751–789, Dec. 2004.

[34] D. E. Thompson *et al.*, "Performance measurement for brain-computer or brain-machine interfaces: A tutorial," *J. Neural Eng.*, vol. 11, no. 3, p. 035001, 2014.

[35] L. H. Smith, T. A. Kuiken, and L. J. Hargrove, "Use of probabilistic weights to enhance linear regression myoelectric control," *J. Neural Eng.*, vol. 12, no. 6, p. 066030, 2015.

[36] J. P. Cunningham, P. Nuyujukian, V. Gilja, C. A. Chestek, S. I. Ryu, and K. V. Shenoy, "A closed-loop human simulator for investigating the role of feedback control in brain-machine interfaces," *J. Neurophysiol.*, vol. 105, no. 4, pp. 1932–1949, Apr. 2011.

[37] R. F. *ff* Weir, P. R. Troyk, G. A. DeMichele, D. A. Kerns, J. F. Schorsch, and H. Maas, "Implantable myoelectric sensors (IMESs) for intramuscular electromyogram recording," *IEEE Trans. Biomed. Eng.*, vol. 56, no. 1, pp. 159–171, Jan. 2009.

[38] A. Ameri, E. N. Kamavuako, E. J. Scheme, K. B. Englehart, and P. A. Parker, "Support vector regression for improved real-time, simultaneous myoelectric control," *IEEE Trans. Neural Syst. Rehabil. Eng.*, vol. 22, no. 6, pp. 1198–1209, Nov. 2014.

[39] E. N. Kamavuako, K. B. Englehart, W. Jensen, and D. Farina, "Simultaneous and proportional force estimation in multiple degrees of freedom from intramuscular EMG," *IEEE Trans. Biomed. Eng.*, vol. 59, no. 7, pp. 1804–1807, Jul. 2012.

[40] J. J. Baker *et al.*, "Decoding individuated finger flexions with Implantable MyoElectric sensors," in *Proc. 30th Annu. Int. Conf. IEEE Eng. Med. Biol. Soc. (EMBS)*, Aug. 2008, pp. 193–196.

[41] P. F. Pasquina *et al.*, "First-in-man demonstration of a fully implanted myoelectric sensors system to control an advanced electromechanical prosthetic hand," *J. Neurosci. Methods*, vol. 244, pp. 85–93, Apr. 2015.

[42] A. d'Avella, P. Saltiel, and E. Bizzi, "Combinations of muscle synergies in the construction of a natural motor behavior," *Nature Neurosci.*, vol. 6, no. 3, pp. 300–308, Mar. 2003.

[43] M. Ortiz-Catalan, B. Hakånsson, and R. Brånemark, "An osseointegrated human-machine gateway for long-term sensory feedback and motor control of artificial limbs," *Sci. Transl. Med.*, vol. 6, no. 257, p. 257re6, Oct. 2014.

[44] D. Farina, K. Yoshida, T. Stieglitz, and K. P. Koch, "Multichannel thin-film electrode for intramuscular electromyographic recordings," *J. Appl. Physiol.*, vol. 104, no. 3, pp. 821–827, Mar. 2008.

[45] S. Muceli *et al.*, "Accurate and representative decoding of the neural drive to muscles in humans with multi-channel intramuscular thin-film electrodes," *J. Physiol.*, vol. 593, no. 17, pp. 3789–3804, Sep. 2015.

[46] C. A. Chestek *et al.*, "Long-term stability of neural prosthetic control signals from silicon cortical arrays in rhesus macaque motor cortex," *J. Neural Eng.*, vol. 8, no. 4, p. 045005, 2011.

[47] W. Bishop *et al.*, "Self-recalibrating classifiers for intracortical brain-computer interfaces," *J. Neural Eng.*, vol. 11, no. 2, p. 026001, 2014.

[48] Z. Li, J. E. O'Doherty, M. A. Lebedev, and M. A. L. Nicolelis, "Adaptive decoding for brain-machine interfaces through Bayesian parameter updates," *Neural Comput.*, vol. 23, no. 12, pp. 3162–3204, Sep. 2011.

[49] E. E. Cavallaro, J. Rosen, J. C. Perry, and S. Burns, "Real-time myoprocessors for a neural controlled powered exoskeleton arm," *IEEE Trans. Biomed. Eng.*, vol. 53, no. 11, pp. 2387–2396, Nov. 2006.

[50] Q. Ding, X. Zhao, A. Xiong, and J. Han, "A novel motion estimate method of human joint with EMG-driven model," in *Proc. 5th Int. Conf. Bioinformatics Biomed. Eng.*, 2011, pp. 1–5.

[51] D. Farina *et al.*, "The extraction of neural information from the surface EMG for the control of upper-limb prostheses: Emerging avenues and challenges," *IEEE Trans. Neural Syst. Rehabil. Eng.*, vol. 22, no. 4, pp. 797–809, Jul. 2014.

[52] L. Firmin *et al.*, "Axon diameters and conduction velocities in the macaque pyramidal tract," *J. Neurophysiol.*, vol. 112, no. 6, pp. 1229–1240, Sep. 2014.

[53] M. Sartori, M. Reggiani, C. Mezzato, and E. Pagello, "A lower limb EMG-driven biomechanical model for applications in rehabilitation robotics," in *Proc. Int. Conf. Adv. Robot.*, 2009, pp. 1–7.

[54] M. H. Schieber, "Individuated finger movements of rhesus monkeys: A means of quantifying the independence of the digits," *J. Neurophysiol.*, vol. 65, no. 6, pp. 1381–1391, Jun. 1991.

[55] J. D. Stewart, "Peripheral nerve fascicles: Anatomy and clinical relevance," *Muscle Nerve*, vol. 28, no. 5, pp. 525–541, Nov. 2003.

[56] A. J. Young, L. J. Hargrove, and T. A. Kuiken, "The effects of electrode size and orientation on the sensitivity of myoelectric pattern recognition systems to electrode shift," *IEEE Trans. Biomed. Eng.*, vol. 58, no. 9, pp. 2537–2544, Sep. 2011.